PAPER • OPEN ACCESS

Feasibility of fusion plasma burn control via real-time, sub-divertor neutral gas isotopic and compositional analysis*

To cite this article: C.C. Klepper *et al* 2025 *Nucl. Fusion* **65** 086015

OPEN ACCESS
IOP Publishing | International Atomic Energy Agency
Nuclear Fusion
Nucl. Fusion **65** (2025) 086015 (17pp)
https://doi.org/10.1088/1741-4326/ade9dc

Feasibility of fusion plasma burn control via real-time, sub-divertor neutral gas isotopic and compositional analysis*

C.C. Klepper[1,], E. Lerche[2], V. Graber[3], E. Delabie[1], E. Schuster[3], T.M. Biewer[1], J.D. Lore[1], P. Jacquet[4], M.J. Mantsinen[5,6], C. Marcus[1], B.R. Quinlan[1], the EUROfusion Tokamak Exploitation Team[a] and JET Contributors[b]**

[1] Oak Ridge National Laboratory, Oak Ridge, TN 37831-6169, United States of America
[2] LPP-ERM/KMS, Royal Military Academy, B-1000 Brussels, Belgium
[3] Lehigh University, Plasma Control Laboratory, Bethlehem, PA 18015, United States of America
[4] United Kingdom Atomic Energy Authority, Culham Science Centre, Abingdon, Oxon OX14 3DB, United Kingdom of Great Britain and Northern Ireland
[5] Barcelona Supercomputing Center, Barcelona, Spain
[6] ICREA, Barcelona, Spain

E-mail: kleppercc@ornl.gov

Received 31 January 2025, revised 31 May 2025
Accepted for publication 30 June 2025
Published 14 July 2025

Abstract

The ability to provide fusion burn control without requiring physical access through the first wall and fuel breeding blankets, would be vital for any future, magnetically confined fusion power reactor. A multi-sensor, fusion fuel cycle exhaust, neutral gas analysis system on JET, capable of delivering real time data, and accessing only the sub-divertor region, provides an excellent example of such capability. Optimized for and operated during the deuterium–tritium experimental campaigns 2 and 3 (DTE2, DTE3), it is proving valuable for planning to explore fusion reactor burn control in ITER with a comparable diagnostic system called the Diagnostic Residual Gas Analyzer (DRGA). This paper aims to show feasibility of developing model-based controllers for ITER and next generation, reactor-relevant devices, by building both on the empirical experience in JET-DTE2, and on the already emerging experience on developing such models specifically for ITER. The paper begins with a specific *use-case* from JET-DTE2, pertaining to the observed sensitivity of the fusion neutron yield on the concentration of isotopic helium-3 (^{3}He), with data from one of the high-performance DT shots exhibited with emphasis on the ^{3}He measurement via the sub-divertor. Then, a first model is developed and then explored

* This manuscript has been authored by UT-Battelle, LLC, under Contract DE-AC05-00OR22725 with the US Department of Energy (DOE). The US government retains and the publisher, by accepting the article for publication, acknowledges that the US government retains a nonexclusive, paid-up, irrevocable, worldwide license to publish or reproduce the published form of this manuscript, or allow others to do so, for US government purposes. DOE will provide public access to these results of federally sponsored research in accordance with the DOE Public Access Plan (http://energy.gov/downloads/doe-publicaccess-plan).
[a] See Joffrin *et al* 2024 (https://doi.org/10.1088/1741-4326/ad2be4) for the EUROfusion Tokamak Exploitation Team.
[b] See Maggi *et al* 2024 (https://doi.org/10.1088/1741-4326/ad3e16) for JET Contributors.
** Author to whom any correspondence should be addressed.

with simulations that aim to discover how well the controllers in the model react to either insufficient levels of ^{3}He or excessive levels of ^{3}He. The simulations then explore potential impact from a delay in the measurement (or the response) that would be comparable to the ~1 s, conductance limited response for the ITER DRGA system, currently in its final design. The simulations show that control is feasible, and that its effectiveness is not significantly impacted by such delay.

Keywords: deuterium–tritium plasmas, diagnostic residual gas analyzer (DRGA), fusion fuel cycle, joint-European torus (JET), magnetic confinement plasmas, ITER, fusion plasma control

(Some figures may appear in colour only in the online journal)

1. Introduction

Plasma control of power producing fusion reactors will need to be based on diagnostic sets that are compatible with the burning plasma environment. The requirements for fuel breeding and energy conversion necessitate maximum utilization of first wall surfaces, which leaves minimal access for diagnostics through the first wall. This is in stark contrast to present-day research devices, which typically have a wide array of diagnostics and access ports to facilitate physics studies. Furthermore, the harsh environment, neutrons, and desire to minimize systems exposed to tritium also all drive towards a reduced diagnostic capability compared to present-day research devices.

The sub-divertor (figure 1) provides a region that is naturally suited for diagnosing core fuel-cycle processes without requiring access through first wall and blankets. The Diagnostic Residual Gas Analyzer (DRGA) that is being designed for the ITER divertor, will sample the sub-divertor region and provide concentrations of hydrogen and helium isotopes, and of seeded impurities at ~1 s response times with respect to changes in the concentration of these species in the that region [1, 2]. Furthermore, current focus on making the DRGA robust enough for use in plasma control for ITER is driving design optimization for the harsh environment of the ITER port cell [3].

One can expect a sub-divertor region to be always present in any reactor design, as it will be needed to provide for a high neutral density region (and therefore high pumping rates) for the particle exhaust part of the fuel cycle, including for He ash removal. As will be seen later, the DRGA combines a special, diagnostic pumping arrangement with two complementary, gas compositional analysis sensors, in configurations that adapt it to the harsh environment while still allowing for response times relevant to fusion plasma exhaust dynamics, e.g. for the ~1 s imposed by formal ITER measurement requirement for the DRGA system for the divertor. (A physics justification for the formal requirement, at least for the fuel gas species, is provided in [1]). By not requiring direct access through the main chamber, such a system as the DRGA, sampling the sub-divertor / pumping ducts would be compatible with commercial reactors from the diagnostics access perspective.

Although it is clearly important to measure the fuel isotopic composition and the helium ash accumulated in the sub-divertor, results from recent and current tokamak experiments have also shown good correlation between core and sub-divertor species concentrations, over plasma—wall equilibration times of a few seconds [4]. This means that the inherent response time of the DRGA is compatible with monitoring species concentration changes in the main plasma and, given its compatibility with the burning plasma environment, suggests the possibility of using the DRGA as a (burning) plasma control diagnostic, with the most promising plasma control *use-cases* including (a) main plasma D/T ratio control, (b) detachment control, (c) core ion heating control, e.g. for T^+ as will be discussed.

However, model-based controllers that are designed to take advantage of this diagnostic have not been developed yet. Model-based controllers use a mathematical model to predict and optimize system behavior. In this case a model describing the response of quantities measurable by diagnostic systems to changes in the fueling and heating actuators, including non-linear effects caused by minority ions, is required for feedback control. This is one of the primary aims of this paper: showing feasibility for the development of such controllers with ITER plasma and burn control as the main application, while using observations from equivalent JET plasmas to conceptually guide this study. As will be discussed, an upgrade of a sub-divertor, neutral gas analysis system ahead of the recent JET deuterium–tritium Experimental Campaigns 2 and 3 (DTE2, DTE3) made that system even more functionally equivalent to the DRGA system under design for ITER. Because it proved so valuable during these JET campaigns, use-case (c), i.e. ion heating control, is also chosen as the ideal one for early exploration of such model-based controllers. This use-case makes optimal use of the DRGA-specific capability to detect species concentrations down to ~1% for hydrogen and 0.1% for He isotopes, both critical for ion cyclotron resonance-frequency heating (ICRH) optimization (see, e.g. examples of both studied for early ITER operation, based on JET studies in [5]).

Thus, the sub-divertor gas analysis system that was especially prepared and optimized for JET-DTE2 [4, 6], and which includes sensors and measurement methods that are prototypical to the ITER DRGA, and its successful deployment during these recent and unique experimental campaigns [2], provides

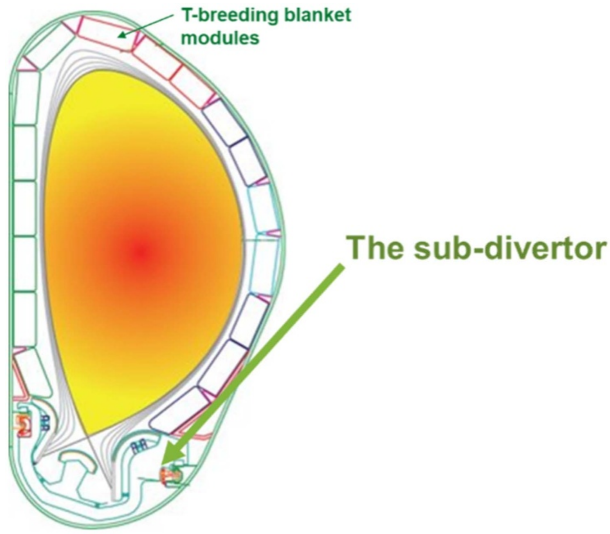

Figure 1. In a fusion reactor, the need for maximum utilization of first wall surfaces for fuel breeding and energy conversion means minimal access for diagnostics through the first wall. as much as 80%–90% of the first wall and possibly the divertor structures would need to be covered by blanket modules [S. Smolentsev, ORNL, Priv. Comm.]. The tokamak cross-section image included in this figure is reproduced with permission from the ITER Organisation.

the impetus for this quest to explore its viability as an ITER and/or future, burning plasma experiment control diagnostic. Of particular interest is this specific application to ^{3}He monitoring for T^+ core heating optimization, which was important in these campaigns for reaching the record DT performance plasmas (see, e.g. [7]), and this will be the primary driver for the present burn control model. It should be noted however that, in these campaigns, the system also had the operations safety function for checking that, when not needed for that specific ICRF heating scheme, residual ^{3}He was kept to an absolute minimum ($<\sim$1% concentration) to avoid damage from spurious ICRF (ion cyclotron range of frequencies) resonances near plasma-facing components (PFCs) that can induce local PFC damage [11].

It will be seen that the JET DT2 campaign can be an invaluable training data source for plasma control exploration of the ITER DRGA. Similarly, one can also envision that ITER will provide immense opportunities to study DRGA-based plasma control for next-step, reactor-relevant fusion devices.

This paper is organized as follows: in section 2, the equivalence of the DRGA implementation for ITER (now in final design) and for JET (as optimized just ahead of JET-DTE2) is highlighted, while the key differences in the configuration of each system's gas composition sensors and pumps are delineated. This is done both to provide the latest update in the design for the ITER DRGA, but also to explain how both systems manage to provide the desired $<$1 s response time for the low mass species, while maintaining operational resilence in the harsh environment that includes magnetic fields up to 250 mT and ionizing radiation doses in the 10^4 to 10^5 Gy range before replacement. In section 3, some specific, DRGA-based plasma control use-cases are considered, and model-based control integration is discussed. In section 4 DRGA-based control models are being explored for the first time. In section 5, controllers are developed based on these models, and simulations are carried out to show feasibility of controlling the DT burn with the DRGA. This last section also includes a repeated simulation but including an assumed 2 s delay, so represent the anticipated, few-sec equilibration time for the sub-divertor neutral species concentrations to match the ones for ion species in the core plasma. In section 6 the outcome of these studies is discussed and conclusions are provided.

2. DRGA implementations for JET-DT and for ITER

As the upgrade of the sub-divertor neutral gas analysis system on JET for DT compatibility ahead of the DTE2 and DTE3 Experimental Campaigns took place in collaboration with the ITER DRGA design team, there are common sensors and methods, as mentioned. Although the system on JET is locally known as 'KT5' the term DRGA will be used for it in this paper, because the two systems are functionally equivalent. The most fundamental difference in DRGA implementation on JET from what is being designed for ITER is that the former is *local*, meaning that the system is physically located under the torus, with the full system input connected directly to the piping that takes the divertor exhaust to the tokamak exhaust system turbo-molecular pumps (TMPs). In this configuration, good response time is assured by this proximity and no intentional conductance (e.g. an orifice) is place at the input of the diagnostic system. In contrast, the ITER implementation has the system (more specifically the analysis station of the system) outside the biological shield to allow for occasional access from maintenance and removal of the system with minimal exposure time for radiation workers and without the need for remote handling. As will be seen, this has required its design to use a novel configuration than includes such a flow restrictive orifice right at the input of full system.

Most importantly, although this *remote* implementation (for ITER, and mostly likely for any future, reactor-like fusion device) means an extra $\sim$8 m of piping (in the case of ITER) from sampling region to the analysis station, the cost in terms of response time is no more that $\sim 3\times$ achieved by the local system on JET. Specifically, the JET system has $\sim$0.3 s response time, while the ITER system will have a $\sim$1 s response time (at least for the fusion process-relevant low-mass species). This means that the remote system still meets the formal ITER design requirements and, as it will be shown further in this paper, is also sufficient for the control of relevant plasma core processes. The two configurations are illustrated in the functional diagrams provided in figure 2. Mechanical models of the two implementations, and further explanation of their design, can be found in [2, 4] respectfully for the ITER and JET systems.

In both configurations shown in figure 2, one notes the presence the two, key and complementary gas composition sensors that are integrated into a DRGA analysis station: the optical gas analyzer (OGA) and the residual gas analyzer (RGA), most

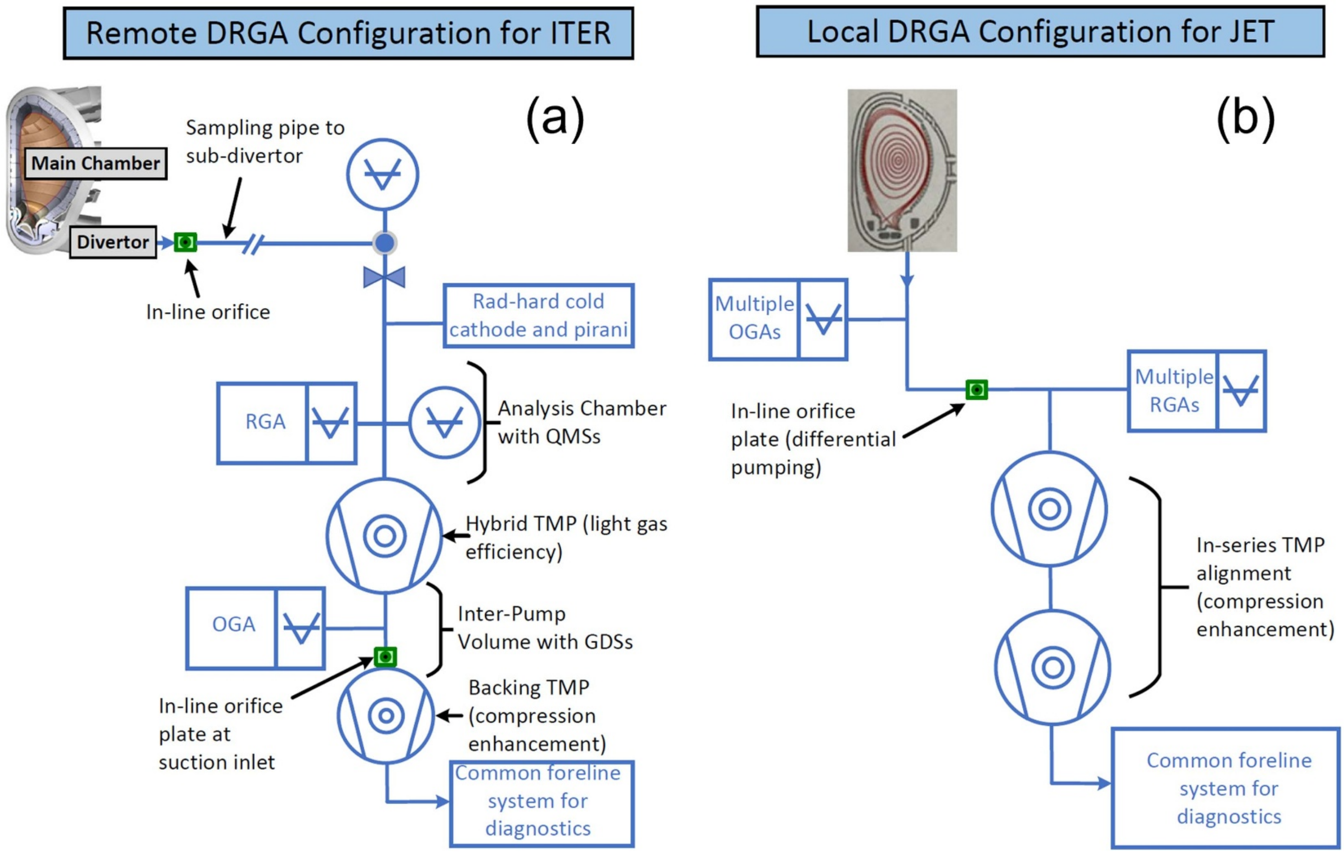

Figure 2. ITER DRGA final design configuration ((*a*), remote) versus JET's upgraded for DT compatibility, functionally equivalent system ((*b*), local). 3D illustration of these systems can be readily found in [2, 6], respectively. In these 2D functional diagrams, RGA denotes the mass spectroscopy part of the DRGA system, and based, in both cases on customized versions of commercial Quadrupole Mass Spectrometers, such as in [8]. OGA denotes the optical gas analysis part of the DRGA measurement, in JET done using Penning discharge plasma sources, as the one illustrated in [9]. For ITER, alternative, not-necessarily Penning-type, Glow Discharge plasma Sources (GDS) are being currently studied, and they will be deployed in the Inter-Pump Volume, as discussed in [10]. The latter reference also explains the additionally novel placement of the second (flow restricting) orifice to maintain optimal pressure for the GDSs, while also mitigating back-streaming of light gases from the (shared) roughing line back into the Inter-Pump Volume, compromising the sensitivity of the OGA measurement. The tokamak cross-section image included in this figure is reproduced with permission from the ITER Organisation.

commonly a quadrupole mass spectrometer (QMS). While in the JET configuration the low-temperature plasma source, which enables spectral emission for the OGA part of the DRGA measurement, is directly exposed to the high neutral pressure environment of the sub-divertor, the ITER design's configuration achieves similarly high pressure by recompressing the effluent neutral gas downstream, using the diagnostic TMPs which are integral to the measurement.

It is worth noting that, while the original innovation that reversed the ordering of RGA to OGA measurement made it possible to achieve this $\sim$1 s response despite the long sampling pipe (see, e.g. in [1]) more recent design innovation allowed for full elimination of light impurity back-streaming into the inter-pump volume, where the OGA measurement takes place in the ITER configuration. This more recent evolution of the design judiciously places an additional orifice in the inter-pump region. Despite this added constriction ahead of the second TMP, lab-based prototyping demonstrated that the modified design can still maintain the $\sim$1 s response time, even in the OGA measurement [10]. As mentioned, this response time is critical in the ability of the DRGA to be responsive to changes in the main plasma, in plasma-wall equilibration times.

3. DRGA-enabled plasma-control solutions

The capability of the DRGA to provide highly reliable measurements of species concentrations in both the divertor and the core makes it suitable for plasma-control applications. Time delays associated with plasma-wall equilibration times must be considered during the synthesis of the controller. Figure 3 illustrates the placement of the DRGA in a control loop with options to be deployed for burn control, divertor control and/or ICRH, as some of the key use-cases.

The limited time of the JET project, from the completion of the system upgrade to the beginning of the last JET experimental campaign (which included pure H and pure T plasma operation, followed by the two rounds of DT operations, i.e. DTE2 and DTE3), did not allow for the development and testing of plasma control based on monitoring changes in the fuel and helium isotopic content via the DRGA-equivalent

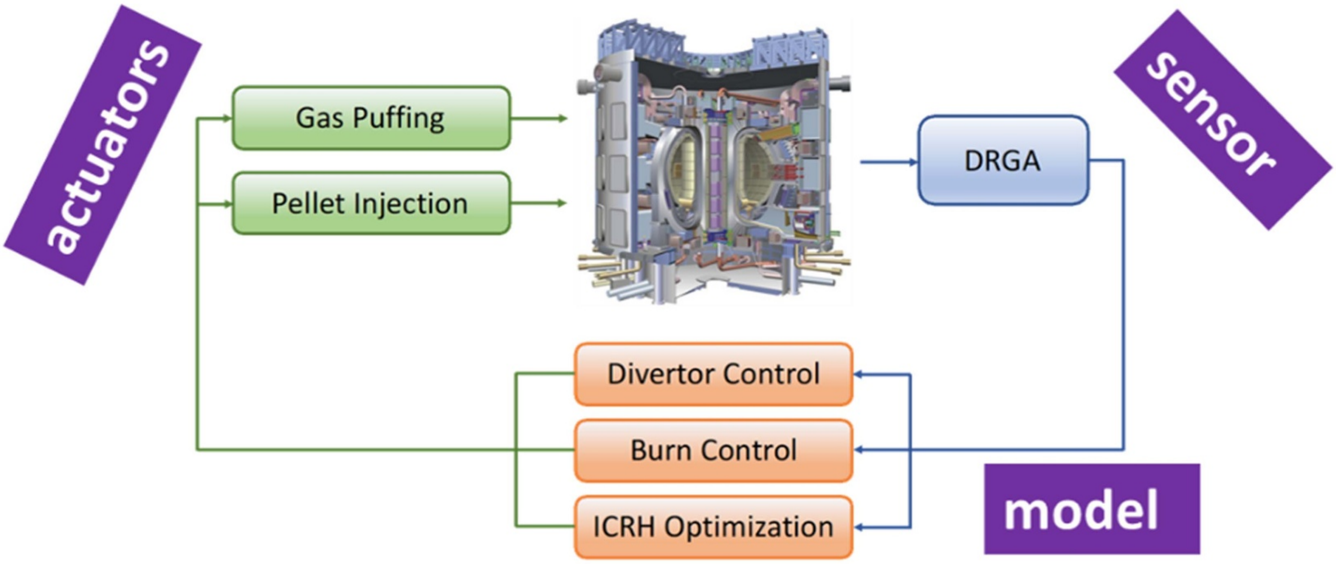

Figure 3. The DRGA can play a critical role in enabling different solutions for burn control, divertor control and ion-cyclotron -resonant-heating optimization. The tokamak cross-section image included in this figure is reproduced with permission from the ITER Organisation.

measurement in the JET sub-divertor. Clearly, this would have been already of interest in view of similar capability being development for ITER. As a substitute for these measurements, real time optical spectroscopy measurements were used to demonstrate feedback control of the Tritium fraction in JET DT plasmas [12].

Furthermore, some aspects of such control were touched upon in [13, 14] ahead of these DT campaigns. Here again, optical spectroscopy inside the main chamber (e.g. divertor spectroscopy) was used for sensing changes in the hydrogen and helium isotopic composition. However, in the case of JET, some of the sightlines could be seen to be influenced by the direct gas fuelling from the divertor and commonly not all sightlines measured the same isotope ratio. In the case of ITER, the much larger broadening predicted for the relevant spectral line emission in the boundary, combined with extra complexity in the fitting and interpretation of the spectra due to larger contributions predicted from reflections off the divertor metal surfaces, will make such measurement nearly unattainable for ITER (see, e.g. related discussion and references in [4]). Therefore the ability to make such measurements in the sub-divertor can be further attractive for ITER despite the longer response time. Nevertheless, although the main motivation of the present work is in support of ITER (and burning plasma fusion devices beyond) it is also driven by the exceptional opportunity to learn as much as possible from the JET DT experience, with its ITER DRGA-equivalent diagnostic, while designing the diagnostic and its plasma control-optimized deployment for these future applications.

Along those lines, the following use-cases for DRGA-based plasma control can be envisioned for ITER, based on the capabilities already exhibited by the JET DRGA and the ones anticipated for the equivalent system on ITER:

3.1. Use-case: burn control by isotopic fueling

Measures of D and T concentrations in the core could enable burn control by isotopically tailored fueling, where the relative mix of DT (tritium fraction γ) is regulated in real time [15]. This is a situation in which an ITER-type DRGA (or equivalent system) would be an ideal sensor.

The fusion power (P_f) in a DT burning plasma is:

$$P_\mathrm{f} = Q_\mathrm{f}\gamma\,(1-\gamma)\,n_\mathrm{DT}^2\langle\sigma\nu\rangle, \tag{1}$$

$$\gamma = \frac{n_\mathrm{T}}{n_\mathrm{DT}}, \tag{2}$$

$$n_\mathrm{DT} = n_\mathrm{D} + n_\mathrm{T}, \tag{3}$$

where $Q_\mathrm{f} = 17.6\,\mathrm{MeV}$, $\langle\sigma\nu\rangle$ is the reactivity, n_T is the tritium density, and n_D is the deuterium density [16]. This burn-control technique becomes particularly relevant as auxiliary heating becomes less efficient in modifying $\langle\sigma\nu\rangle$ given the magnitude of the fusion heating.

This control solution demands independent D and T pellet injectors. These will be the actuators in a control loop as in figure 3.

3.2. Use-case: divertor protection by particle control

Measures of fuel and impurity concentrations in the divertor/SOL region could enable divertor protection by optimally regulating the amounts of boundary radiation and divertor detachment. Neon (Ne) is a typical radiative cooling ‘additive’ in the fuel cycle mix and it can be also measured/monitored by the DRGA. The same is true of Argon (Ar) which was found in DTE3 to work well in this respect when seeded together with Ne, as recently reported [17].

The actuators in such a control solution would be fuel and impurity puffing systems. It is worth pointing out that that the timescales for control relevant for avoiding MARFEs (multi-faceted asymmetric radiation from the edge) and rapid reattachment are much too fast for this control, but the DRGA could potentially be used to modify, for example, the degree of detachment given a stable and broad operational window.

3.3. Use-case: ICRH optimization by ^{3}He control

^{3}He minority heating and 2nd harmonic heating of T are the two main ICRH schemes foreseen for ITER full-field operation in D–T plasmas; they were successfully applied in JET-DTE2 to enhance core plasma heating (supplementing NBI) and thus DT burn [7]. As will be illustrated in section III.D, the supplemental heating is strongly sensitive to the ^{3}He concentration. (The heated ^{3}He ions then efficiently transfer their energy to the T^+ ions, which have the same mass). Thus, real-time measurement and control of ^{3}He concentrations could enable optimization of ICRH by optimally regulating heating efficiency and contributing in this way to effective plasma heating and burn control. The fact that this could be done with a DRGA-based sensor results from recent demonstration on JET that, with only minor optimization of existing JET-DRGA hardware, it was possible to resolve ^{3}He from ^{4}He and reliably measure ^{3}He/(D+T) with a fraction of 1% detection limit [9].

The key actuator for this control solution would be an independent ^{3}He puffing system.

3.4. Model-based control integration

All these control use-cases (burn control, divertor control, ICRH optimization) are strongly coupled. An actuator commanded by one controller affects plasma states regulated by other controllers. An integrated control solution demands a model-based design combining core/divertor fueling and heating [18]. Such an integrated solution could leverage simultaneous measurement of multiple species concentrations by DRGA, including H, D, T, ^{3}He, ^{4}He, Ne, to name a few key ones already in the requirements for the ITER DRGA.

Along these lines, an integrated control solution strongly based on the very recently demonstrated ^{3}He detection capability for the DRGA makes an ideal focus for the present study, which aims to show feasibility for DRGA-based plasma control. One important reason for this is that the recent JET-DT experience with ITER DRGA prototypical sensors and methods provides already evidence of DT burn sensitivity to ^{3}He concentration, as monitored with the JET-DRGA. This is seen, for instance, in figure 4, in which relevant signals from one of the performance plasmas of the DTE2 campaign are plotted.

In the figure, top panel to bottom panel, one sees (*a*) the total neutral beam power, which is the primary source of auxiliary power and is nearly the same in the two plasma pulses, and the ICRH power, with antenna power modulated in the late part of one of the pulses; (*b*) the line averaged electron density, also similar in the two pulses; (*c*) the resulting ^{3}He concentrations, as determined from the sub-divertor measurement, plotted in the same panel with the ^{3}He injection program time traces (i.e. the dashed lines of the same corresponding colors) which are different for the two pulses; (*d*) the neutron rate, which is an indicator of DT fusion burn, and showing a peak value at the time marked by the vertical dashed line; (*e*) the total energy content of the plasma discharge; and (*f*) the central ion temperature from charge-exchange spectroscopy. Although both (*e*) and (*f*) show a peak value at the time when the ^{3}He concentration is at 2%, the effect is most notable in the neutron rate signal.

This peaking of the neutron rate is understood as resulting from a competition between fuel dilution by the added ^{3}He, which would decrease DT fusion performance, and ICRH ion heating (also from increased ^{3}He concentration) which would tend to increase DT fusion performance DT fusion performance. Optimum for achieving highest neutron rate is around 2% for these tow, high- performance JET-DTE2 plasma discharges. Although in this present study, a control model is being explored for ITER (in the future) and not for JET (which has now permanently shutdown) the plot in figure 4 clearly shows the sensitivity of DT burn to ^{3}He concentration, and motivates the present study given that this ICRH heating scheme is expected to be deployed also for ITER.

In further support of the significance of the application for integrated control model, it is noted that ICRH is of interest both for pre-DT and for DT operations on ITER, providing not only additional heating of core plasma ions, but also a barrier to W accumulation in the core [19]. In JET-DTE2, the ICRH heating scheme based on small concentrations of ^{3}He was shown to be quite effective in heating ions in JET DT plasmas and thus promising for similar impact in ITER DT operations. In the same experimental campaign, the same OGA that will be integral to the ITER DRGA was shown to provide reliable ^{3}He concentration measurements down to fractions of 1%. This is important both in the mentioned ICRH scheme for DT plasmas, but also as a safety measurement, when it is important to reduce ^{3}He down below 1% to avoid spurious resonances near the boundary layer (typically at the outer wall, in the presence of ^{3}He) that can damage PFCs [9, 11]. No other diagnostic can measure this species at such low concentrations.

4. A first exploration of DRGA-based control model options

As discussed in the previous section, ‘real life’ data from JET-DTE2 clearly highlight the sensitivity of the burn on ^{3}He concentration, which we can anticipate in ITER operation with similar ICRH coupling scheme implemented to provide additional heating to the T ions. An example of the ICRF power absorbed per species expected in ITER DT operation is shown in figure 5 as function of the ^{3}He concentration. These results were obtained with the 1D TOMCAT code, as in [22] but extended to DT plasmas, assuming a 50:50 DT mix with $B_o = 5.3$ T and ICRF frequency $f = 52$ MHz. The solid (black) line represents the total single pass absorption of the ICRF wave, which indicates the global heating efficiency of this ICRF scheme as function of the ^{3}He concentration.

With these numbers at hand, a DRGA-enabled, nonlinear burn controller is then constructed from a control-oriented plasma model. This controller regulates the plasma energy and

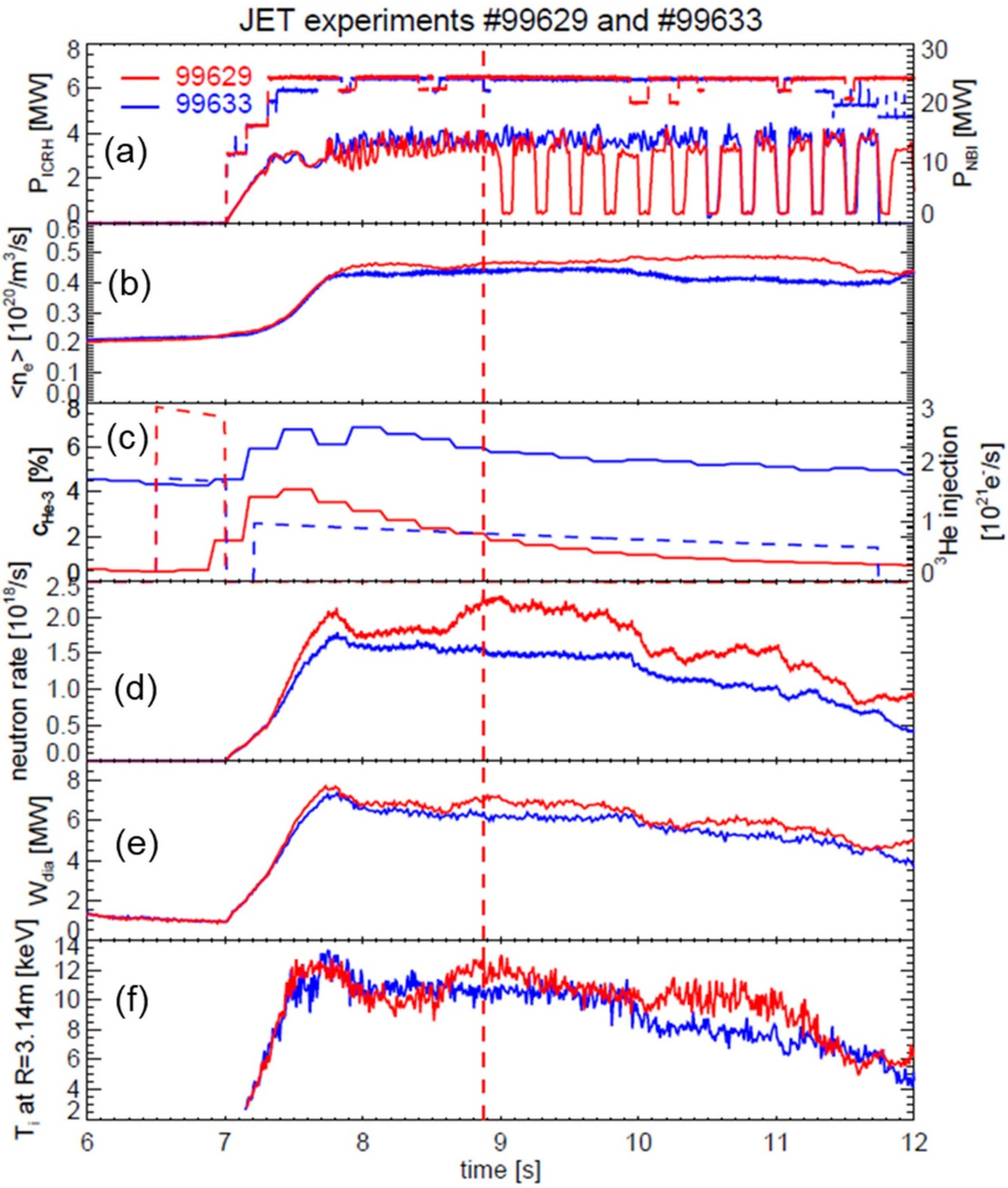

Figure 4. Data from two JET plasma pulses using ^{3}He and 2nd harmonic T heating [7, 11]. (*a*) NBI power, in dashed lines, and the ICRH power, in solid lines; (*b*) n_e, central sightline averaged; (*c*) the ^{3}He injection program, in dashed lines, and the resulting ^{3}He concentrations, as determined from the sub-divertor OGA measurement, shown in solid lines; (*d*) the neutron rate, which is an indicator of DT fusion burn; (*e*) the total energy content; and (*f*) the central ion temperature. The dashed vertical line indicates the time at which 2% ^{3}He is reached in JET Pulse 99 629; this time is clearly coincident with a substantial peaking in the neutron rate; there is also peaking in the central ion temperature, albeit not as clear as in the neutrons signal. The other JET pulse (99 633) exhibits always much higher ^{3}He concentration and it is clearly missing this peaking in fusion burn that is enabled with the added heating from this ^{3}He based ICRH coupling scheme for these JET-DT scenarios.

density by making requests for auxiliary power and external fueling. These control requests are satisfied using the following actuator systems: neutral beam heating, ion cyclotron heating and DT pellet injection. If these actuator systems saturate, the controller will not be able to achieve the reference targets for the plasma energy and density. Taking advantage of real-time measurements from the DRGA, this burn controller includes a policy to dynamically compensate for ICRF power saturation. If the ICRF power saturates, the controller will automatically regulate the ^{3}He concentration in the plasma's core using ^{3}He gas puffing from the mid-plane valve. By modulating the ^{3}He gas injection rate, the controller increases or decreases the ^{3}He concentration such that the ICRF power absorption is improved in accordance to figure 5. With the improved ICRF power absorption, the power output of the ICRF system will desaturate,

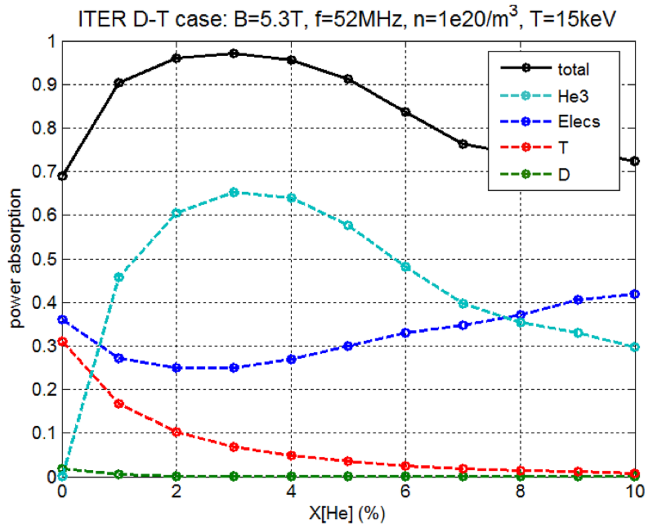

Figure 5. ICRH power absorption curves from TOMCAT simulations. It is noted that while this code has not been formally validated against JET DT data, it has been validated against data from JET pure D plasma and, more recently, against WEST tokamak D plasmas, as indicated in [20, 21], respectively.

allowing the controller to drive the plasma to the reference targets.

For the controller and the associated simulations, the key measurement for the ^{3}He gas injection actuator is the DRGA. As mentioned, it is providing the concentration of ^{3}He in the sub-divertor (in terms of the neutral gas composition there) which is assumed to correspond to the concentration in the main plasma (in terms of the ion concentrations there) albeit with a delay that depends on plasma-wall equilibration. The modeling study then also explores the potential impact of this delay on the ability to provide this control function with the DRGA. The DRGA also provides measurements for the concentrations of the other ion species including deuterium, tritium and alpha-particles.

In the remainder of this section, the burning plasma model, from which the nonlinear controller was synthesized, is presented. This model captures the highly nonlinear and coupled dynamics of the plasma's ion energy, electron energy and the density of each of the ion species. Furthermore, this plasma model is used to run the closed-loop simulations presented in section 5.2.

4.1. Density response models

In this burning plasma model, there are five ion species: deuterium (D), tritium (T), alpha particles (denoted as α or ^{4}He), helium-3 (^{3}He), and an additional impurity with atomic number Z_I. Respectively, their densities n_D, n_T, n_α, n_He3, and n_I are governed by

$$\dot{n}_\mathrm{D} = -\frac{n_\mathrm{D}}{\tau_\mathrm{D}} - S_\alpha + S_\mathrm{D}^\mathrm{rec} + S_\mathrm{D}^\mathrm{inj}, \tag{4}$$

$$\dot{n}_\mathrm{T} = -\frac{n_\mathrm{T}}{\tau_\mathrm{T}} - S_\alpha + S_\mathrm{T}^\mathrm{rec} + S_\mathrm{T}^\mathrm{inj}, \tag{5}$$

$$\dot{n}_\alpha = -\frac{n_\alpha}{\tau_\alpha} + S_\alpha, \tag{6}$$

$$\dot{n}_\mathrm{He3} = -\frac{n_\mathrm{He3}}{\tau_\mathrm{He3}} + S_\mathrm{He3}^\mathrm{gas}, \tag{7}$$

$$\dot{n}_\mathrm{I} = -\frac{n_\mathrm{I}}{\tau_\mathrm{I}} + S_\mathrm{I}^\mathrm{sp}, \tag{8}$$

where each term is expressed in units of $\mathrm{m}^{-3}\mathrm{s}^{-1}$. The pellet injectors fuel deuterium (4) and tritium (5) at controlled rates of $S_\mathrm{D}^\mathrm{inj}$ and $S_\mathrm{T}^\mathrm{inj}$, respectively. Assuming that there are two pellet injectors,

$$S_\mathrm{D}^\mathrm{inj} = (1-\gamma_{\mathrm{p}_1})\, S_1^\mathrm{pel} + (1-\gamma_{\mathrm{p}_2})\, S_2^\mathrm{pel}, \tag{9}$$

$$S_\mathrm{T}^\mathrm{inj} = \gamma_{\mathrm{p}_1} S_1^\mathrm{pel} + \gamma_{\mathrm{p}_2} S_2^\mathrm{pel}, \tag{10}$$

where S_1^pel and S_2^pel are the fueling rates from the two pellet injectors, and γ_{p_1} and γ_{p_2} are the tritium fractions of the pellets sourced from their respective injectors. In (7), the controlled injection rate of ^{3}He is given by $S_\mathrm{He3}^\mathrm{gas}$, which is assumed to come from the mid-plane gas valve.

Due to plasma-wall interactions, there exists uncontrolled wall-recycling sources for deuterium and tritium that are given by $S_\mathrm{D}^\mathrm{rec}$ and $S_\mathrm{T}^\mathrm{rec}$ in (4) and (5). The Z_I-impurity also has an uncontrolled wall-sputtering source S_I^sp. These three wall sources are given by

$$S_\mathrm{D}^\mathrm{rec} = \frac{f_\mathrm{eff}}{1-f_\mathrm{ref}\,(1-f_\mathrm{eff})} \left\{ f_\mathrm{ref}\frac{n_\mathrm{D}}{\tau_\mathrm{D}} + \left(\frac{n_\mathrm{D}}{\tau_\mathrm{D}} + \frac{n_\mathrm{T}}{\tau_\mathrm{T}}\right) \times \left(1-\gamma^\mathrm{PFC}\right) \left[\frac{(1-f_\mathrm{ref}\,(1-f_\mathrm{eff}))\,R^\mathrm{eff}}{1-R^\mathrm{eff}\,(1-f_\mathrm{eff})} - f_\mathrm{ref}\right]\right\}, \tag{11}$$

$$S_\mathrm{T}^\mathrm{rec} = \frac{f_\mathrm{eff}}{1-f_\mathrm{ref}\,(1-f_\mathrm{eff})} \left\{ f_\mathrm{ref}\frac{n_\mathrm{T}}{\tau_\mathrm{T}} + \left(\frac{n_\mathrm{D}}{\tau_\mathrm{D}} + \frac{n_\mathrm{T}}{\tau_\mathrm{T}}\right) \times \gamma^\mathrm{PFC} \left[\frac{(1-f_\mathrm{ref}\,(1-f_\mathrm{eff}))\,R^\mathrm{eff}}{1-R^\mathrm{eff}\,(1-f_\mathrm{eff})} - f_\mathrm{ref}\right]\right\}, \tag{12}$$

$$S_\mathrm{I}^\mathrm{sp} = f_\mathrm{I}^\mathrm{sp}\left(\frac{n}{\tau_\mathrm{I}} + \dot{n}\right), \tag{13}$$

where R^{eff} is the global recycling coefficient, f_{eff} is the recycled-particle fueling efficiency, f_{ref} is the fraction of escaping particles that are reflected back into the plasma, γ^{PFC} is the recycled particles' tritium fraction, and f_{I}^{sp} is the sputtering fraction. A derivation for the particle recycling terms (11) and (12) is provided in [18].

The DT reaction rate density, which depends on the reactivity $\langle\sigma\nu\rangle$, is given by

$$S_\alpha = n_{\text{D}} n_{\text{T}} \langle\sigma\nu\rangle. \tag{14}$$

With the ion temperature T_{i} expressed in keV,

$$\langle\sigma\nu\rangle = C_1\omega\sqrt{\xi/\left(m_{\text{r}}c^2T_{\text{i}}^3\right)}\mathrm{e}^{-3\xi}, \quad \xi = \left(B_{\text{G}}^2/4\omega\right)^{1/3} \tag{15}$$

$$\omega = T_i\left[1 - \frac{T_i\left(C_2 + T_i\left(C_4 + T_iC_6\right)\right)}{1 + T_{\text{i}}\left(C_3 + T_{\text{i}}\left(C_5 + T_{\text{i}}C_7\right)\right)}\right]^{-1}, \tag{16}$$

where the constants B_{G}, $m_{\text{r}}c^2$ and C_j for $j\in\{1,\ldots,7\}$ can be found in [23].

In (4)–(8), τ_{D}, τ_{T}, τ_α, τ_{He3}, and τ_{I} are the particle confinement times. The plasma's tritium fraction γ and the DT density n_{DT} are given by (2) and (3) in section 3. Respectively, the total ion density n_{i}, the electron density n_{e}, and the effective atomic number Z_{eff} are given by

$$n_{\text{i}} = n_{\text{DT}} + n_\alpha + n_{\text{He3}} + n_{\text{I}}, \tag{17}$$

$$n_{\text{e}} = n_{\text{DT}} + 2n_\alpha + 2n_{\text{He3}} + Z_{\text{I}}n_{\text{I}}, \tag{18}$$

$$Z_{\text{eff}} = \frac{n_{\text{DT}} + 4n_\alpha + 4n_{\text{He3}} + Z_{\text{I}}^2n_{\text{I}}}{n_{\text{e}}}, \tag{19}$$

where (18) is the quasi-neutrality condition. The total plasma density is sum of the ion and electron densities: $n = n_{\text{i}} + n_{\text{e}}$.

4.2. Energy response models

All of the ion species are assumed to share the same temperature (T_{i}), which is distinct from the temperature of the electrons (T_{e}). The response models for the ion energy ($E_i = \frac{3}{2}n_{\text{i}}T_{\text{i}}$) and the electron energy ($E_{\text{e}} = \frac{3}{2}n_{\text{e}}T_{\text{e}}$) are

$$\dot{E}_{\text{i}} = -\frac{E_{\text{i}}}{\tau_{\text{E,i}}} + \phi_\alpha P_\alpha + P_{\text{ei}} + P_{\text{aux,i}}, \tag{20}$$

$$\dot{E}_{\text{e}} = -\frac{E_{\text{e}}}{\tau_{\text{E,e}}} + (1-\phi_\alpha)P_\alpha - P_{\text{ei}} - P_{\text{br}} + P_{\text{oh}} + P_{\text{aux,e}}, \tag{21}$$

where each term is in units of W m^{-3}. The alpha-particle heating is given by $P_\alpha = Q_\alpha S_\alpha$ where $Q_\alpha = 3.52$ MeV, and the fraction of P_α that is deposited into the plasma's ion population is ϕ_α (the remainder heats the electrons).

The bremsstrahlung radiation losses, the ohmic heating, and the ion-electron collisional power exchange are given by

$$P_{\text{br}} = 5.5\times10^{-37}Z_{\text{eff}}n_{\text{e}}^2\sqrt{T_{\text{e}}[\text{keV}]}, \tag{22}$$

$$P_{\text{oh}} = 2.8\times10^{-9}Z_{\text{eff}}I_{\text{p}}^2a^{-4}\left(T_{\text{e}}[\text{keV}]\right)^{-3/2}, \tag{23}$$

$$P_{\text{ei}} = \frac{3}{2}n_{\text{e}}\frac{T_{\text{e}} - T_{\text{i}}}{\tau_{\text{ei}}}, \tag{24}$$

where I_{p} and a are the plasma current and minor radius. The energy relaxation time [24] is

$$\tau_{\text{ei}} = \frac{3\pi\sqrt{2\pi}\varepsilon_0^2T_{\text{e}}^{3/2}}{e^4m_{\text{e}}^{1/2}\ln\Lambda_{\text{e}}}\sum_{\text{ions}}\frac{m_{\text{p}}}{n_{\text{p}}Z_{\text{p}}^2}, \tag{25}$$

where $e = 1.622\times10^{-19}$ C, $m_{\text{e}} = 9.1096\times10^{-31}$ kg, and $\varepsilon_0 = 8.854\times10^{-12}$ F m^{-1}. The natural logarithm is defined as $\Lambda_k = 1.24\times10^7T_k^{3/2}/(n_{\text{e}}^{1/2}Z_{\text{eff}}^2)$ for $k\in\{\text{i},\text{e}\}$. The summation, which includes the ion mass m_p and the atomic number Z_{p}, is taken over all of the ion species: $p\in\{\text{D},\text{T},\alpha,\text{He3},\text{I}\}$. In (20) and (21), the ion and electron energy confinement times are represented by $\tau_{\text{E,i}}$ and $\tau_{\text{E,e}}$.

ITER's various plasma-heating actuator systems deliver powers $P_{\text{aux,i}}$ and $P_{\text{aux,e}}$ to the ions and electrons, respectively. In this work, the auxiliary heating methods include neutral beam injection (NBI) and ion cyclotron range of frequencies (ICRF) heating such that

$$P_{\text{aux,i}} = \phi_{\text{ic,i}}P_{\text{ic}} + \phi_{\text{nb}}\eta_{\text{nb}}P_{\text{nb}}, \tag{26}$$

$$P_{\text{aux,e}} = \phi_{\text{ic,e}}P_{\text{ic}} + (1-\phi_{\text{nb}})\eta_{\text{nb}}P_{\text{nb}}, \tag{27}$$

where P_{nb} and P_{ic} are the injected NBI and ICRF powers, respectively. The fraction ϕ_{nb} of the NBI power is delivered to the ions, while the remainder is delivered to the electrons. The overall heating efficiency of the NBI is $\eta_{\text{nb}}\leqslant1$. The amount of ICRF power that is absorbed by the ions and the electrons ($\phi_{\text{ic,i}}$ and $\phi_{\text{ic,e}}$) is a function of the ^{3}He concentration

$$\text{X[He3] }(\%) = \frac{n_{\text{He3}}}{n_{\text{e}}}\times100, \tag{28}$$

as defined by figure 5. In figure 5, the fraction of the ICRF power absorbed by the electrons is given by the blue curve ($\phi_{\text{ic,e}}$), and the black curve defines the total ICRF power absorption by the entire plasma (i.e. the ICRF heating efficiency). Therefore, the ICRF power absorbed by the ions ($\phi_{\text{ic,i}}$) can be found by subtracting the blue curve from the black curve. In (26) and (27), a term for the overall heating efficiency of the ICRF system ($\eta_{\text{ic}}\leqslant1$) is not included because the data presented in figure 5 already incorporates it.

Both the alpha-particle power (P_α) and the neutral beam power (P_{nb}) heat the plasma by introducing highly kinetic 'fast ions' that collide with the surrounding plasma particles [16]. As discussed above, these fast ions deposit a fraction, denoted as ϕ_f for $f\in\{\alpha,nb\}$, of their energy into the plasma's ion population, while the remainder goes to the plasma's electron population. A derivation of the following formula can be found in [25]:

$$\phi_f = \frac{1}{x_0}\left[\frac{1}{3}\ln\frac{1-x_0^{\frac{1}{2}}+x_0}{\left(1+x_0^{\frac{1}{2}}\right)^2} + \frac{2}{\sqrt{3}}\left(\tan^{-1}\frac{2x_0^{\frac{1}{2}}-1}{\sqrt{3}}+\frac{\pi}{6}\right)\right], \tag{29}$$

where $x_0 = \varepsilon_{f_0}/\varepsilon_c$ is the ratio between the fast ion's initial kinetic energy and the critical energy. The critical energy [26]

$$\varepsilon_c = m_e^{-1/3}A_f\frac{T_e}{n_e^{2/3}}\left(\frac{3\sqrt{\pi}\ln\Lambda_i}{4\ln\Lambda_e}\right)^{2/3}\left(\sum_{ions}\frac{n_pZ_p^2}{A_p}\right), \tag{30}$$

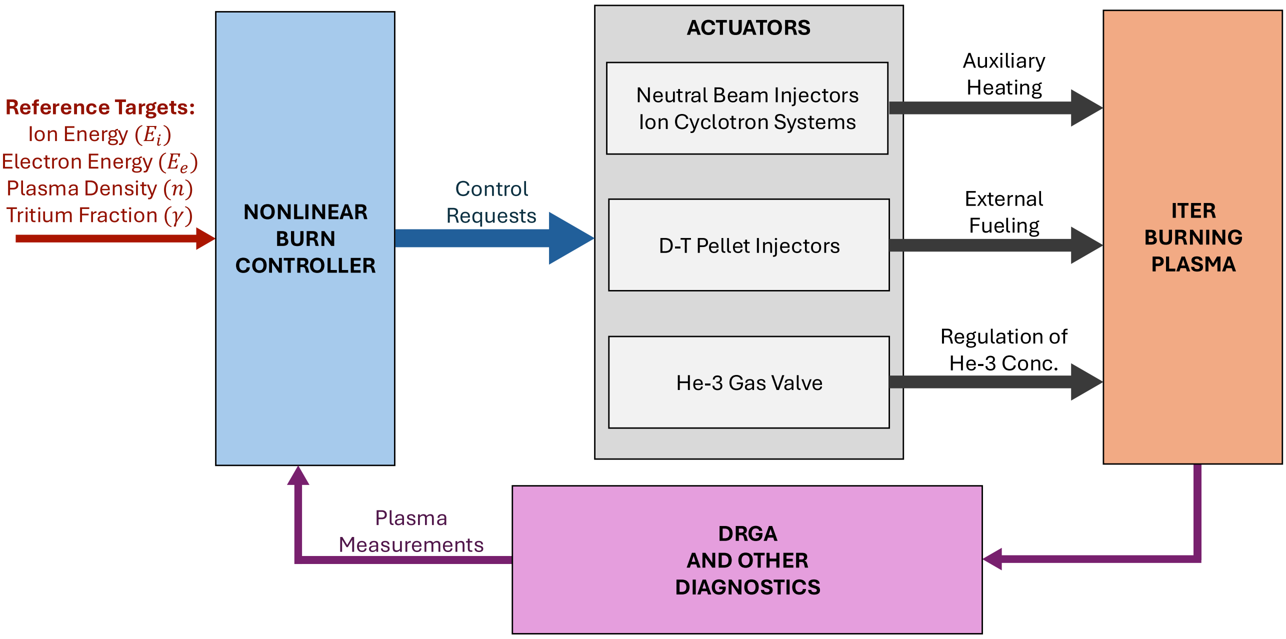

Figure 6. Using measurements provided by the DRGA and other diagnostics, the burn controller computes the auxiliary ion power ($\bar{P}_{\mathrm{aux,i}}$), auxiliary electron power ($\bar{P}_{\mathrm{aux,e}}$), external deuterium injection ($\bar{S}_{\mathrm{D}}^{\mathrm{inj}}$), and external tritium injection ($\bar{S}_{\mathrm{T}}^{\mathrm{inj}}$) that will drive the plasma towards the reference targets for the ion energy (E_{i}), electron energy (E_{e}), plasma density (n), and tritium fraction (γ). These control requests are then mapped to the outputs of the actuators: the ICRF power (P_{ic}), the neutral beam power (P_{nb}), and the fueling rates of the two pellet injectors (S_1^{pel} and S_2^{pel}). If P_{ic} or P_{nb} saturate at their maximum or minimum values, then He-3 gas puffing ($S_{\mathrm{He3}}^{\mathrm{gas}}$) is employed to modulate the He-3 concentration. This changes the ICRF power absorption such that the actuator power desaturates and the plasma can be driven to the reference targets.

depends on the atomic mass of the fast ion A_f for $f\in\{\alpha, nb\}$ and the atomic mass of each of the ion species A_p for $p\in\{D,T,\alpha,\mathrm{He3},I\}$. Also, m_{e} is expressed in amu in (30). For the calculation of ϕ_α using (29) and (30), the initial kinetic energy is $\varepsilon_{\alpha_0}=Q_\alpha$ and the atomic mass of an alpha-particle is $A_\alpha=4$. ITER's NBI system will use deuterium particles with 1 MeV of kinetic energy [27]. Therefore, ϕ_{nb} is computed using $\varepsilon_{\mathrm{nb}_0}=1$ MeV and $A_{\mathrm{nb}}=2$.

The confinement times shown in (4)–(8) and (20), (21) are assumed to be directly proportional to the global energy confinement time τ_{E}. Therefore, $\tau_{\mathrm{E,i}}=\zeta_{\mathrm{E,i}}\tau_{\mathrm{E}}$, $\tau_{\mathrm{E,e}}=\zeta_{\mathrm{E,e}}\tau_{\mathrm{E}}$, and $\tau_{\mathrm{p}}=\zeta_{\mathrm{p}}\tau_{\mathrm{E}}$ for $p\in\{\mathrm{D},\mathrm{T},\alpha,\mathrm{He3},I\}$ where $\zeta_{E,i}$, $\zeta_{E,e}$, and ζ_{p} for $p\in\{\mathrm{D},\mathrm{T},\alpha,\mathrm{He3},I\}$ are constant. The IPB98(y,2) scaling law for the global energy confinement time [28] can be written as

$$\tau_{\mathrm{E}}=0.0562\times HKP_{\mathrm{tot}}^{-0.69}V^{-0.69}n_{\mathrm{e}}^{0.41}, \tag{31}$$

where H is the H-factor, V is the plasma volume, n_{e} is in units of 10^{19} m^{-3}, and the total plasma power (MW m^{-3}) is

$$P_{\mathrm{tot}}=P_{\mathrm{aux,i}}+P_{\mathrm{aux,e}}+P_\alpha+P_{\mathrm{oh}}-P_{\mathrm{br}}. \tag{32}$$

In (31), $K=I_{\mathrm{p}}^{0.93}B_{\mathrm{T}}^{0.15}M^{0.19}R^{1.97}\epsilon^{0.58}\kappa^{0.78}$ where B_{T} is the toroidal field, R is the plasma major radius, $\epsilon=a/R$, κ is the vertical elongation at 95% flux surface, and $M=3\gamma+2(1-\gamma)$. Respectively, I_p, B_T, R, a, κ and V are equal to 15 MA, 5.3 T, 6.2 m, 2 m, 1.7, and 837 m^3 for ITER operation.

5. Findings from the exploratory, DRGA-based control model simulations

5.1. Burn control design

To illustrate the potential of using the DRGA for burn control applications, a nonlinear burn controller was designed using the plasma model presented in section 4. This Lyapunov-based controller [29] is similar to the designs presented in prior works [30, 31] except that it exploits the dependence the ICRF power absorption on the ^{3}He concentration in the plasma's core, which is measurable due to the DRGA. By controlling the ^{3}He gas injection ($S_{\mathrm{He3}}^{\mathrm{gas}}$) into the plasma, the controller can regulate the helium-3 concentration (28) such that the ICRF power absorption is either increased or decreased in accordance with figure 5. Therefore, $S_{\mathrm{He3}}^{\mathrm{gas}}$ can be used to regulate the plasma energy. Because the control synthesis is similar to the aforementioned prior works, particularly [30], details on the design of the control algorithm have been omitted from this work. A step-by-step derivation of the controller discussed here, which is used in the simulation study presented in section 5.2, can be found in [32].

Figure 6 presents a diagram of the closed-loop system. Using control laws that are computed with measurements from the DRGA and other diagnostic tools, the controller determines the amounts of external deuterium injection ($\bar{S}_{\mathrm{D}}^{\mathrm{inj}}$), external tritium injection ($\bar{S}_{\mathrm{T}}^{\mathrm{inj}}$), auxiliary ion heating ($\bar{P}_{\mathrm{aux,i}}$) and auxiliary electron heating ($\bar{P}_{\mathrm{aux,e}}$) necessary to drive the plasma dynamics towards user-defined reference targets for the ion

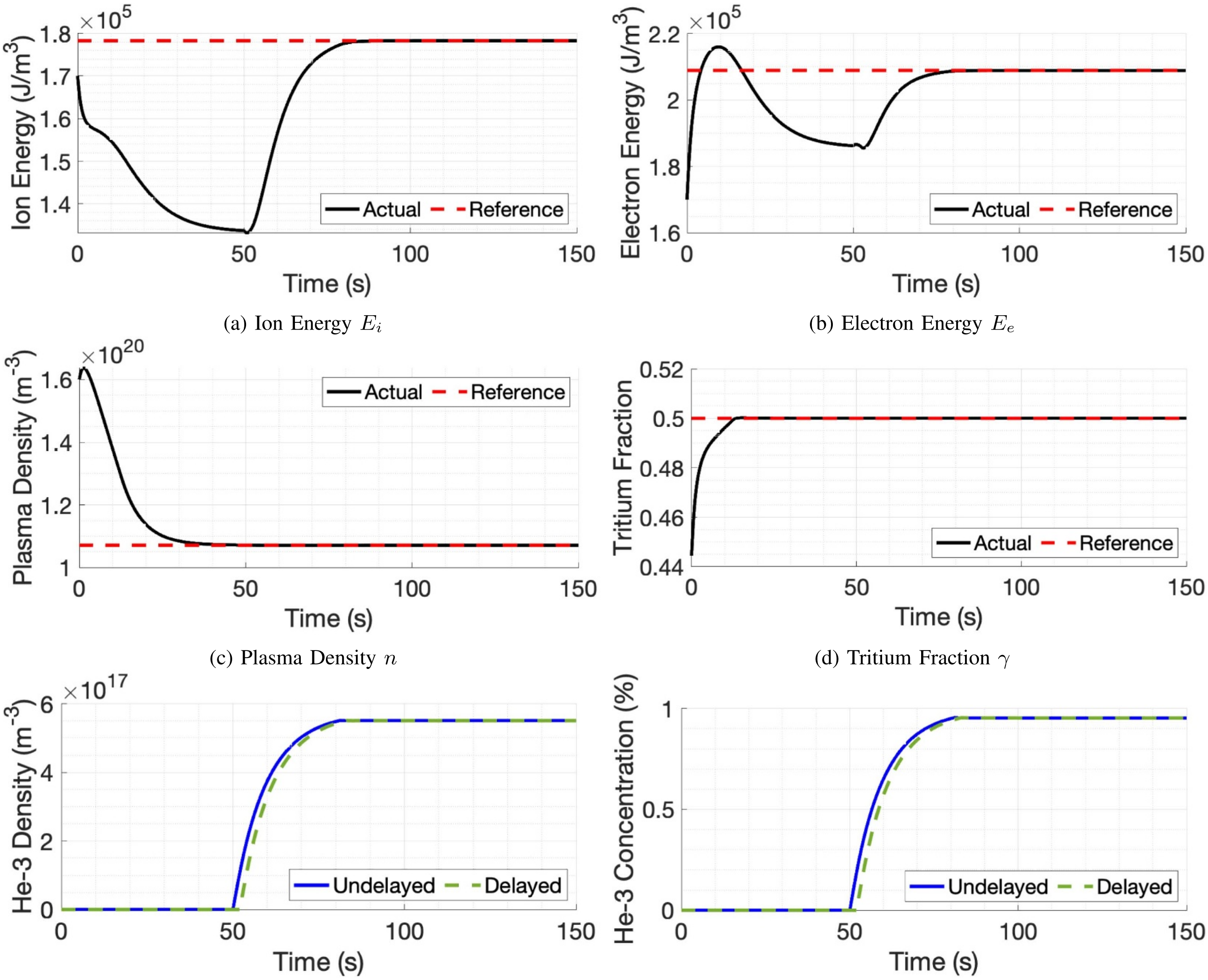

(a) Ion Energy E_i

(b) Electron Energy E_e

(c) Plasma Density n

(d) Tritium Fraction γ

(e) He-3 Density n_{He3}

(f) He-3 Conc. X[He3]

Figure 7. (*a*)–(*d*) The reference tracking for E_i, E_e, n, and γ is shown. It is unsuccessful for $t < 50$ s because of the saturation of the ICRF power. The reference tracking only succeeds after the He-3 gas injection is activated at $t = 50$ s. (*e*), (*f*) This is caused by the increase in the He-3 concentration, which improves the plasma's ICRF power absorption. [Simulation #1].

energy density E_i, electron energy density E_{e}, total plasma density n and tritium fraction γ. These control requests are mapped to the pellet injectors, ICRF systems and the neutral beam injectors using (9), (10), (26) and (27). Because there are four control requests ($\bar{S}_{\mathrm{D}}^{\mathrm{inj}}$, $\bar{S}_{\mathrm{T}}^{\mathrm{inj}}$, $\bar{P}_{\mathrm{aux,i}}$ and $\bar{P}_{\mathrm{aux,e}}$) and four actuators (S_1^{pel}, S_2^{pel}, P_{ic} and P_{nb}), the required output of each of the actuators can be solved immediately for the given control requests. If there were more actuators than control requests, which would be the case if electron cyclotron heating was also considered, then an allocation algorithm would be required to optimally map the actuator outputs to the control requests. Such an algorithm was presented in prior work [31], but it is excluded from this work for the sake of brevity.

If the ICRF power (P_{ic}) or the NBI power (P_{nb}) saturate at their maximum or minimum values, then the actuators will fail to produce the controller's requests for external heating. In other words, the auxiliary power produced by the actuators ($P_{\mathrm{aux,i}}$ and $P_{\mathrm{aux,e}}$ from (26) and (27)) will not match the amounts requested by the controller ($\bar{P}_{\mathrm{aux,i}}$ and $\bar{P}_{\mathrm{aux,e}}$). As a result, the plasma system will not be driven to the reference targets. To overcome this obstacle, the controller is designed to automatically change the ^{3}He concentration using helium-3 gas injection ($S_{\mathrm{He3}}^{\mathrm{gas}}$) in order to desaturate the auxiliary power, allowing the control requests to be met ($P_{\mathrm{aux,i}} = \bar{P}_{\mathrm{aux,i}}$ and $P_{\mathrm{aux,e}} = \bar{P}_{\mathrm{aux,e}}$). With the control requests satisfied, the plasma system can be driven to the reference targets.

5.2. *Simulation study*

In this section, the potential of DRGA-enabled burn control is illustrated in a simulation study. Using the controller described in section 5.1, two closed-loop simulations of the burning

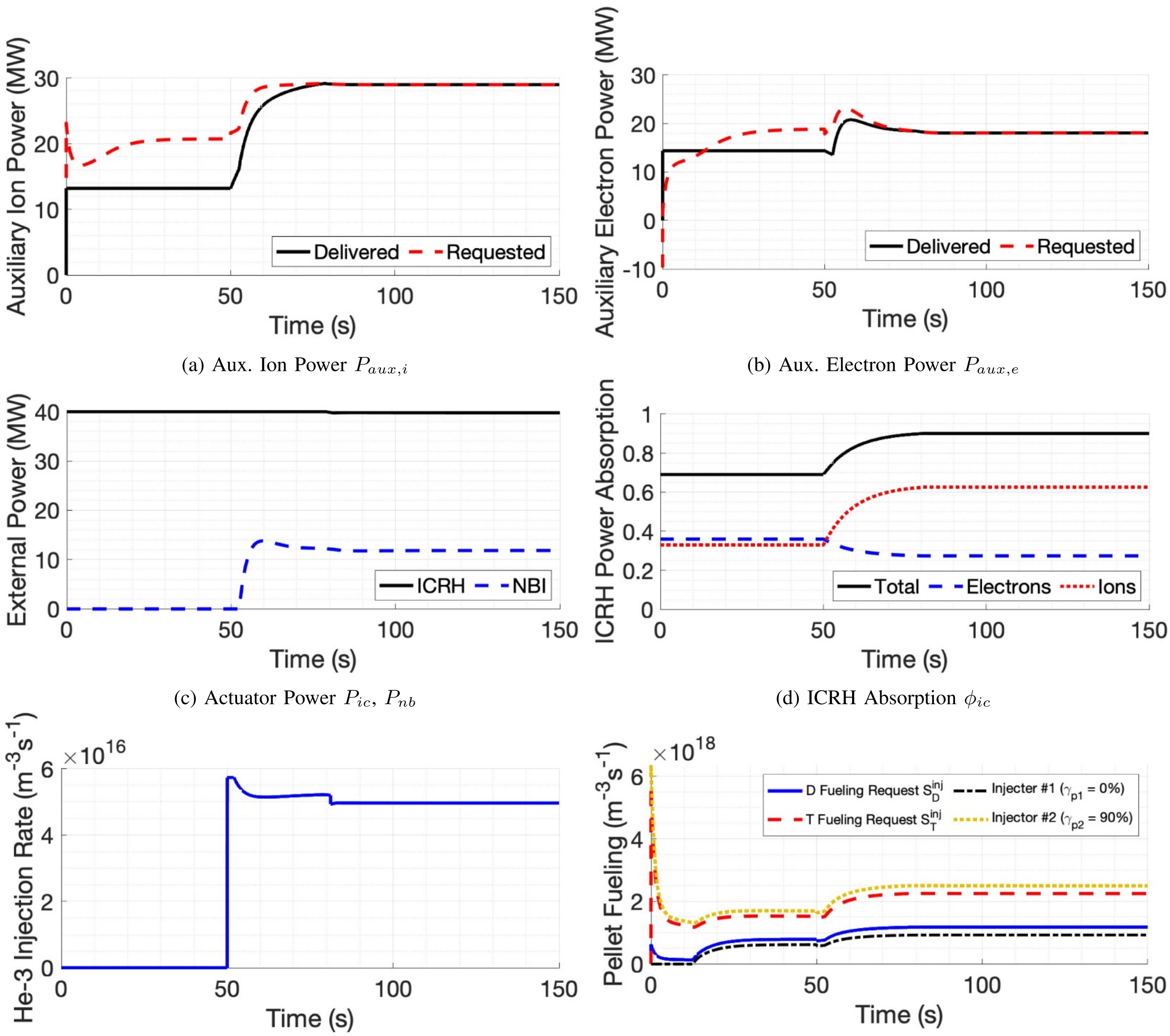

(a) Aux. Ion Power $P_{aux,i}$

(b) Aux. Electron Power $P_{aux,e}$

(c) Actuator Power P_{ic}, P_{nb}

(d) ICRH Absorption ϕ_{ic}

(e) He-3 Injection S_{He3}^{gas}

(f) Ext. Fueling S_D^{inj}, S_T^{inj}

Figure 8. (*a*) and (*b*) The auxiliary power requested by the controller versus the auxiliary power produced by the actuators. (*c*) The power output of the ICRF and NBI systems. (*d*) The ICRF power absorption (determined by the results in figure 5). (*e*) The gas puffing rate for He-3. (*f*) The controller's requests for external DT fueling and the output of the pellet injectors. **[Simulation #1]**.

plasma model (section 4) were completed. In both simulations, the controller aims to drive the plasma to the following reference targets: $E_{\mathrm{i}} = 1.78 \times 10^5\ \mathrm{J\,m^{-3}}$, $E_{\mathrm{e}} = 2.09 \times 10^5\ \mathrm{J\,m^{-3}}$, $\gamma = 0.5$ and $n = 1.07 \times 10^{20}\ \mathrm{m^{-3}}$. The two simulations share the same initial conditions and model parameters. In regard to the plasma confinement properties, H, $\zeta_{\mathrm{E,i}}$, $\zeta_{\mathrm{E,e}}$, ζ_{D}, ζ_{T}, ζ_{α}, ζ_{He3} and ζ_I were set to 1.1, 1.2, 1.05, 4, 2, 4, 4 and 5, respectively. In regard to the particle sources from the walls, $R^{\mathrm{eff}} = 0.7$, $f_{\mathrm{eff}} = 0.4$, $f_{\mathrm{ref}} = 0.6$, $\gamma^{\mathrm{PFC}} = 0.65$ and $f_I^{\mathrm{sp}} = 0.02$. The saturation point for the NBI and ICRF power output (P_{nb} and P_{ic}) were both set to 40 MW. For the pellet injection, $\gamma_{\mathrm{p1}} = 0\%$ and $\gamma_{\mathrm{p2}} = 90\%$. Finally, $\eta_{\mathrm{nb}} = 95\%$ and $Z_{\mathrm{I}} = 4$.

The setup for the two simulations differ in one aspect only. In simulation #1, the helium gas injection is forced to be zero for the first 50 s of the simulation ($S_{\mathrm{He3}}^{\mathrm{gas}} = 0$ for $t < 50$ s) such that the helium-3 density remains at its initial condition of zero ($n_{\mathrm{He3}} = 0$ for $t < 50$ s). In Simulation #2, $S_{\mathrm{He3}}^{\mathrm{gas}} = 3.5 \times 10^{17}\ \mathrm{m^{-3}s^{-1}}$ for $t < 50$ s such that the ^{3}He density climbs to a high value. In both simulations, this is done so that the ^{3}He concentration is at a value that corresponds to poor ICRF power absorption in the plasma. With the optimal ^{3}He concentration being 3% according to figure 5, the ^{3}He concentration is too low in the beginning of Simulation #1 and too high in the beginning of Simulation #2. With the poor ICRF

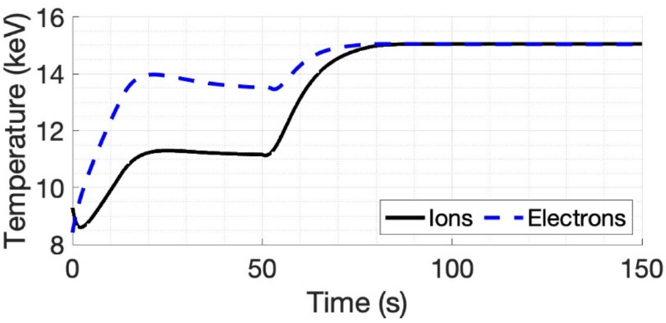

(a) Temperature T_i, T_e

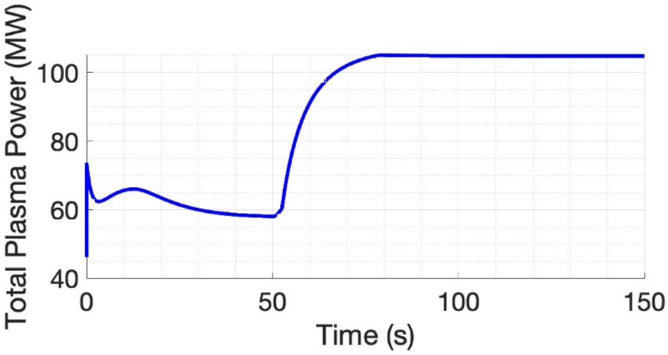

(b) Total Power P_{tot}

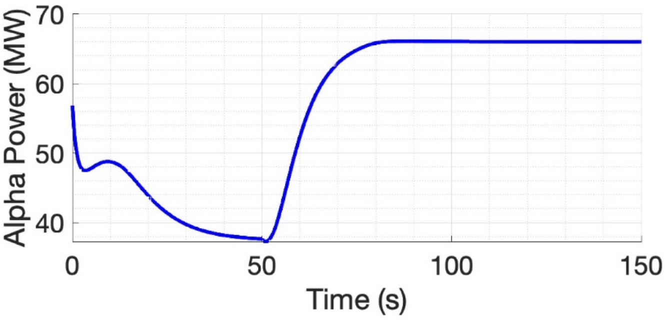

(c) Alpha Power P_α

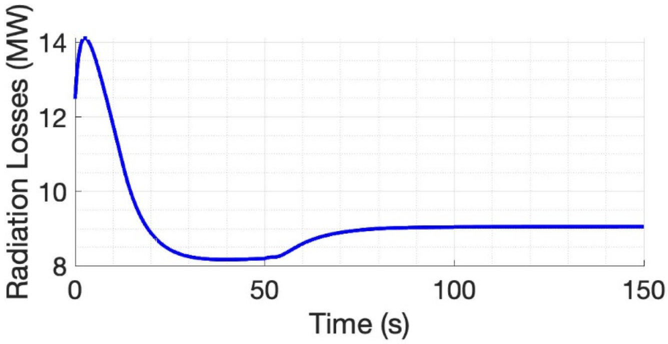

(d) Radiation Power P_{br}

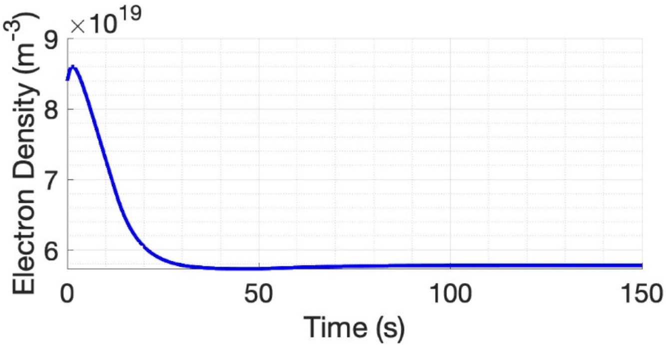

(e) Electron Density n_e

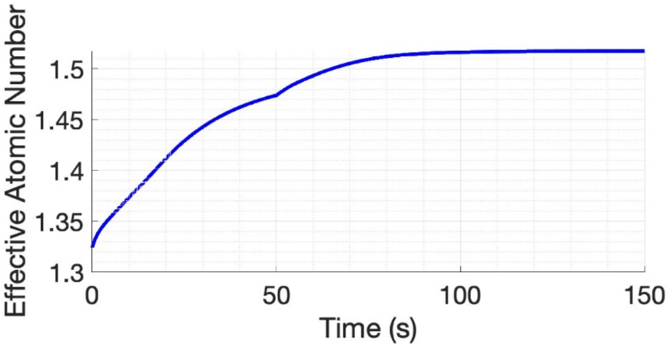

(f) Eff. Atomic Number Z_{eff}

Figure 9. (*a*) The ion and electron temperatures. (*b*)–(*d*) The total plasma power, the alpha-particle power and the radiation power. (*e*), (*f*) The electron density and the effective atomic number. **[Simulation #1]**.

power absorption, the ICRF power saturates ($P_{\mathrm{ic}} = 40$ MW) in the beginning of both simulations. After $t = 50$ s, $S^{\mathrm{gas}}_{\mathrm{He3}}$ is no longer forced to be a fixed value, permitting the controller to increase or decrease $S^{\mathrm{gas}}_{\mathrm{He3}}$ to control the ^{3}He concentration. In both simulations, the controller automatically computes the necessary change in the ^{3}He concentration that would improve the ICRF power absorption enough to desaturate P_{ic}.

In addition to studying the potential of ^{3}He gas injection for controlling the plasma energy, it is also of interest to explore the impact of the DRGA response time, especially for the remote system to be deployed in the ITER divertor where the response time is $\sim$1 s for the fuel cycle, low atomic mass species and somewhat higher for the radiate cooling gases. To study this, a two-second delay is applied to all DRGA-relevant measurements received by the controller. This includes the density and concentration of all of the ion species in the plasma's core: deuterium, tritium, alpha-particles, and ^{3}He.

The results of simulation #1 are shown in figures 7–9. In the beginning of the simulation where $S^{\mathrm{gas}}_{\mathrm{He3}} = 0$ for $t < 50$ s, the ion and electron energies (E_{i} and E_{e}) fail to reach their reference targets. The cause for this can be seen in figures 8(*a*) and (*b*). One can see that the control requests for the external heating ($P_{\mathrm{aux,i}}$ and $P_{\mathrm{aux,e}}$) cannot be delivered because the ICRF power (P_{ic}) saturates at 40 MW (figure 8(*c*)), i.e. reached the maximum power that can be supplied by the external RF electronics (sources, transmission lines and RF matching circuits) without having coupled the desired energies into the main plasma. This is then the cause of the problem that triggers the following solution once the controller is permitted to modulate $S^{\mathrm{gas}}_{\mathrm{He3}}$ at $t = 50$ s: the controller automatically computes the ^{3}He

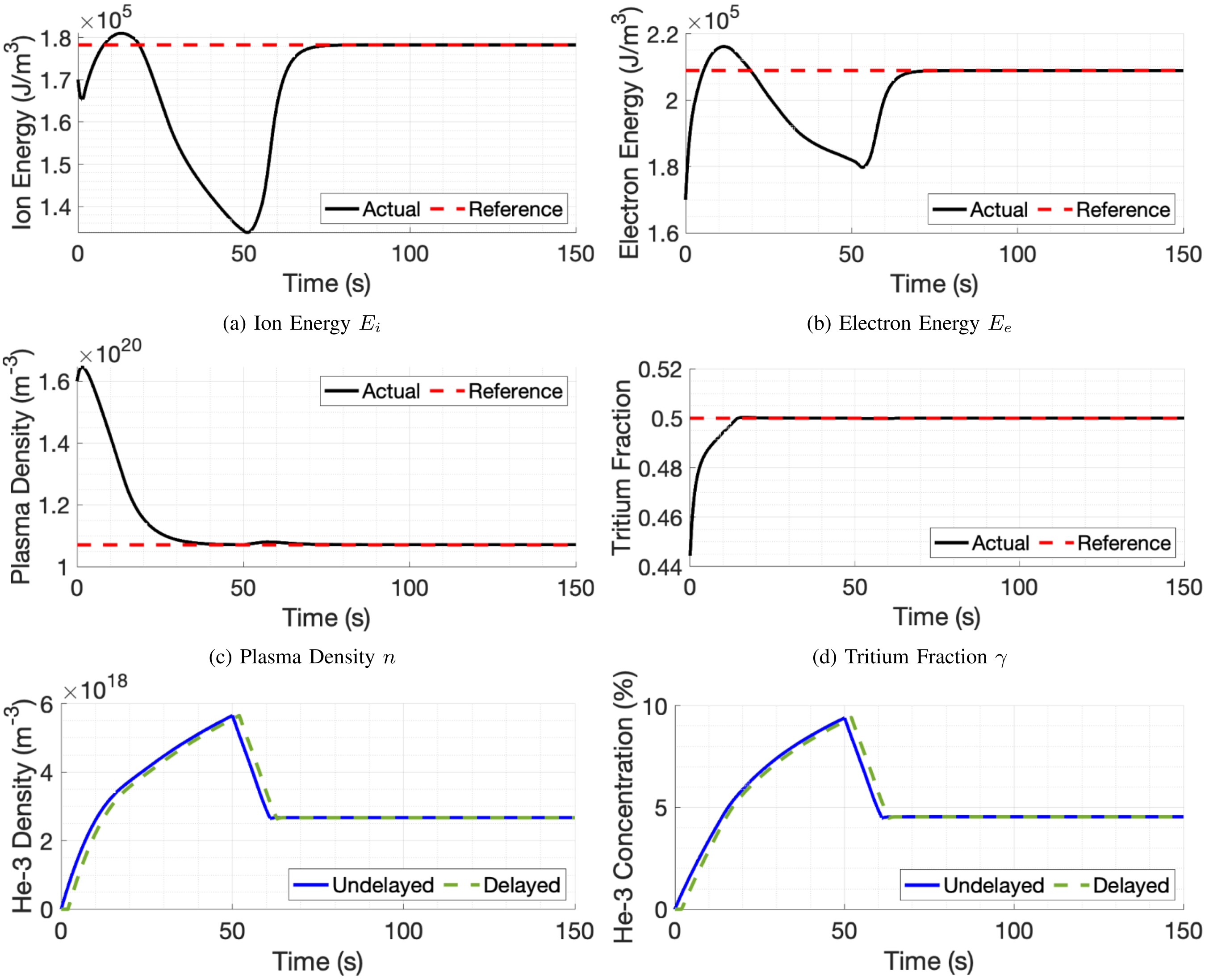

(a) Ion Energy E_i

(b) Electron Energy E_e

(c) Plasma Density n

(d) Tritium Fraction γ

(e) He-3 Density n_{He3}

(f) He-3 Conc. X[He3]

Figure 10. (*a*)–(*d*) The reference tracking for E_{i}, E_{e}, n, and γ is shown. It is unsuccessful for $t < 50$ s because of the saturation of the ICRF power. The reference tracking only succeeds after the He-3 gas injection is activated at $t = 50$ s. (*e*), (*f*) This is caused by the increase in the He-3 concentration, which improves the plasma's ICRF power absorption. **[Simulation #2]**.

concentration that will improve the ICRF power absorption enough to desaturate the ICRF power. The controller responds by changing the injection level (increasing in this example) of ^{3}He into the plasma. As shown in figure 7(*f*), the controller increases the ^{3}He concentration from 0% to 0.95%.

As a result of this change, E_{i} and E_{e} reach their reference targets. Looking at the resulting effect in more detail, in figure 7, one sees that the total ICRF power absorption increases from 69% to 90%, with absorption by the ions increasing from 33% to 63%, while the absorption by the electrons decreases from 36% to 27%. The result is a desaturation of the ICRF power, allowing the actuators to deliver the requested $P_{\mathrm{aux,i}}$ and $P_{\mathrm{aux,e}}$. In addition to regulating the plasma energy, the controller also drives n and γ to their reference targets (see figures 7(*c*) and (*d*)) despite the two-second delay applied to the ion density measurements. Finally, important plasma conditions, including the alpha-particle power and the electron density, are plotted in figure 9.

The key observations of simulation #2 are similar to simulation #1. Figures 10–12 show the results of simulation #2, where $S^{\mathrm{gas}}_{\mathrm{He3}} = 3.5 \times 10^{17}$ m^{-3}s^{-1} for $t < 50$ s. For $t < 50$ s, the ^{3}He concentration climbs from 0% to a maximum of 9.18%

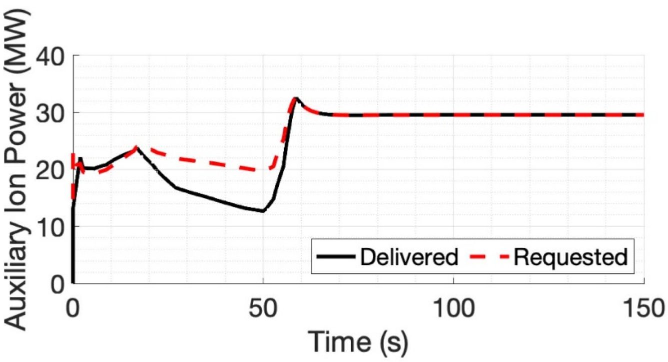

(a) Aux. Ion Power $P_{aux,i}$

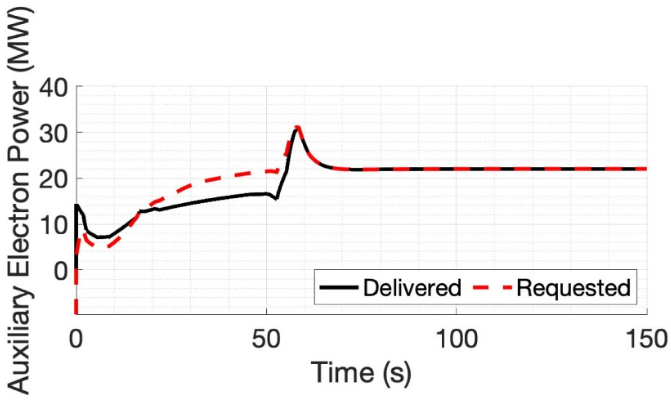

(b) Aux. Electron Power $P_{aux,e}$

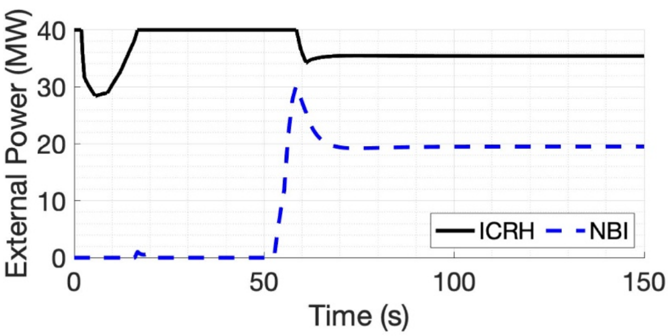

(c) Actuator Power P_{ic}, P_{nb}

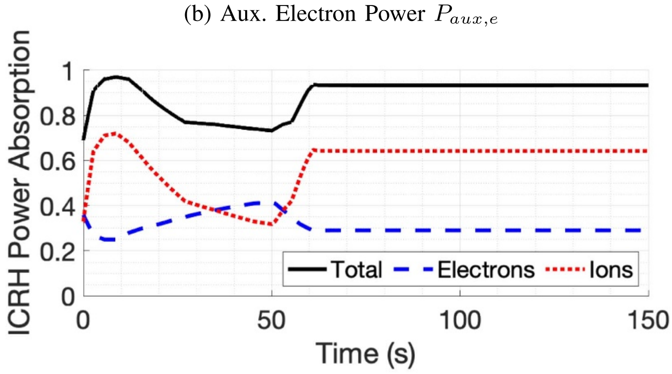

(d) ICRH Absorption ϕ_{ic}

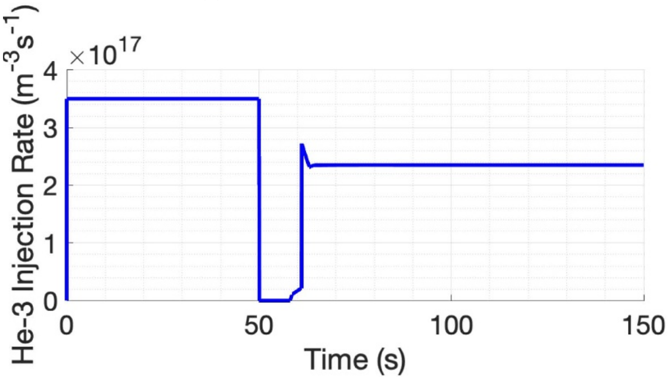

(e) He-3 Injection S^{gas}_{He3}

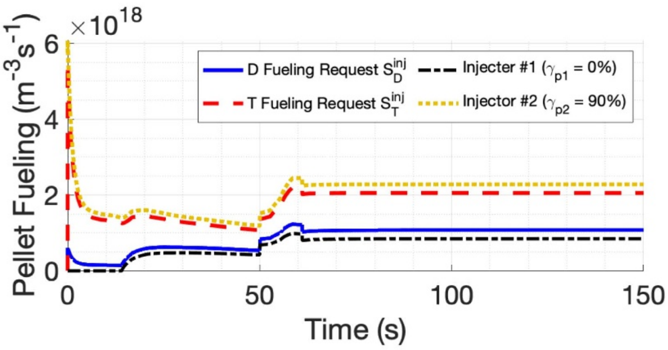

(f) Ext. Fueling S_D^{inj}, S_T^{inj}

Figure 11. (*a*) and (*b*) The auxiliary power requested by the controller versus the auxiliary power produced by the actuators. (*c*) The power output of the ICRF and NBI systems. (*d*) The ICRF power absorption (determined by the results in figure 5). (*e*) The gas puffing rate for He-3. (*f*) The controller's requests for external DT fueling and the output of the pellet injectors. **[Simulation #2]**.

(see figure 10(*f*)). As shown in figure 11(*c*), the ICRF power starts the simulation at the maximum saturation point of 40 MW, desaturates for a brief window when the ^{3}He concentration becomes more favorable, and saturates again once the ^{3}He concentration becomes too high for efficient ICRF power absorption.

Because the ICRF power is saturated at $t = 50$ s, the controller cannot achieve its reference targets for the plasma energy (figures 10(*a*) and (*b*)). Once the controller is given control of the helium gas injection at $t = 50$ s, it lowers the injection rate (figure 11(*e*)) such that the ^{3}He concentration drops to 4.54%. This causes the total ICRF power absorption to increase from 73% to 93%, the absorption by the ions to increase from 32% to 64%, and the absorption by the electrons to decrease from 41% to 29% (figure 11(*d*)). As a result, the ICRF power (figure 11(*c*)) desaturates, and E_i and E_e are driven to their reference targets (figures 10(*a*) and (*b*)). The total plasma density and the tritium fraction (figures 10(*c*) and (*d*)) are also brought to their reference targets despite the DRGA measurement delays. Finally, figure 12 shows other quantities that may be of interest, including the temperature and the radiation losses.

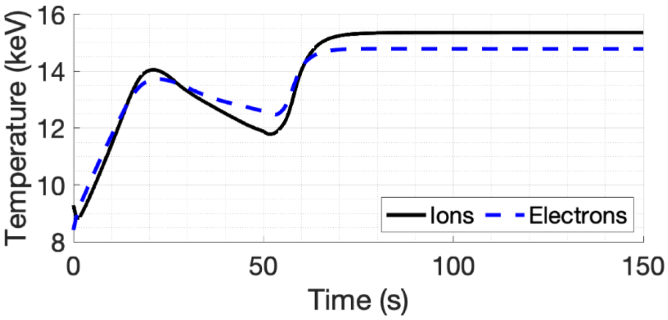

(a) Temperature T_i, T_e

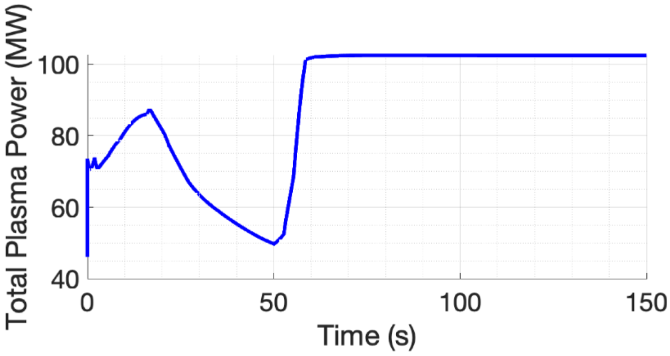

(b) Total Power P_{tot}

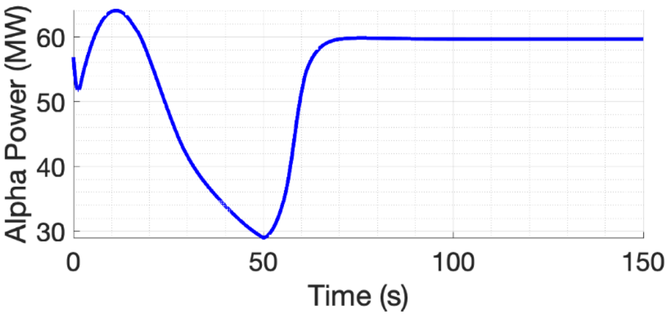

(c) Alpha Power P_α

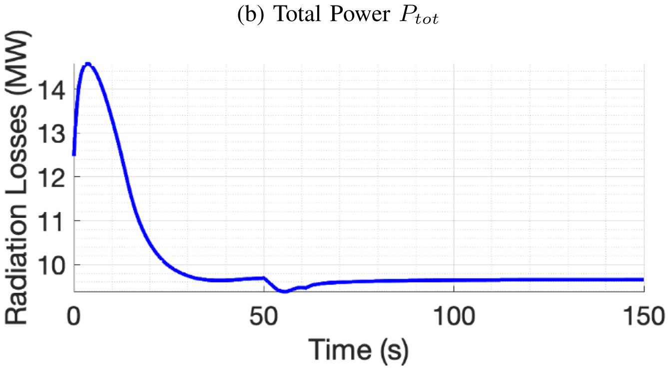

(d) Radiation Power P_{br}

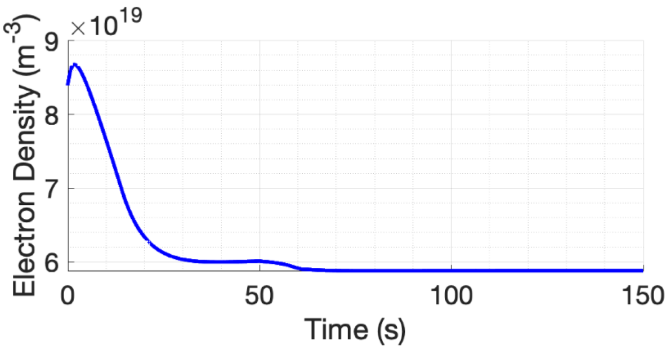

(e) Electron Density n_e

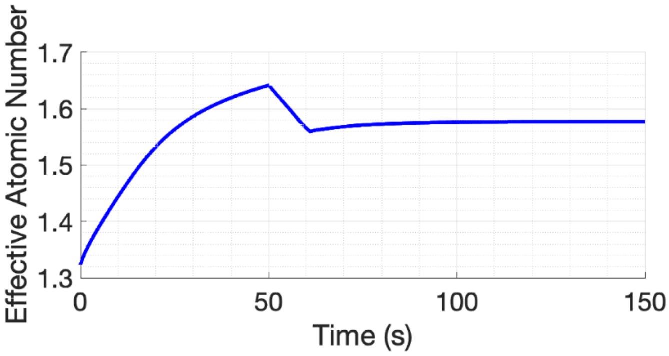

(f) Eff. Atomic Number Z_{eff}

Figure 12. (*a*) The ion and electron temperatures. (*b*)–(*d*) The total plasma power, the alpha-particle power and the radiation power. (*e*)–(*f*) The electron density and the effective atomic number. **[Simulation #2]**.

6. Discussion and conclusions

Regarding the exploration of potential impact from a 1 s delay based on the ITER divertor DRGA system design, it should be recalled that the equilibration between plasma core and sub-divertor, in terms of gas species and isotopic composition, is expected to be of the order of several seconds [4]. Thus, it is not the design of this diagnostic system but the inherent time to bring the wall, including the sub-divertor region into equilibrium that would produce such 'delay' for the effect of the controllers. Nevertheless, it is encouraging to see, in these exploratory simulations, the impact is negligible and, therefore, this study clears the way for the feasibility of reactor environment-compatible, DRGA-based control, at least for this first, ITER DT phase-relevant, core heating use-case.

Acknowledgments

Valuable conversations with Drs. P.C. de Vries and M. Schneider, of the ITER Organization, motivating the pursuit of this study in it early stages, are gratefully acknowledged. This work has been carried out within the framework of the EUROfusion Consortium, funded by the European Union via the Euratom Research and Training Programme (Grant Agreement No 101052200 – EUROfusion). Views and opinions expressed are however those of the author(s) only and do not necessarily reflect those of the European Union (EU) or the European Commission (EC). Neither the EU nor the EC can be held responsible for them. This work has been part-funded by the EPSRC Energy Programme [Grant Number EP/W006839/1]. This work has been funded in part by the US Department of

Energy (DOE), under Contract DE-AC05-00OR22725 with UT-Battelle, LLC.

References

[1] Klepper C. *et al* 2015 Design of a diagnostic residual gas analyzer for the ITER divertor *Fusion Eng. Des.* **96–97** 803–7
[2] Klepper C.C. *et al* 2022 Developments and challenges in the design of the ITER DRGA *IEEE Trans. Plasma Sci.* **50** 4970–9
[3] Quinlan B.R., Marcus C., Biewer T.M., Jugan A.S. and Klepper C.C. 2024 Design considerations to ensure robustness of the ITER diagnostics residual gas analyzer *IEEE Trans. Plasma Sci.* **52** 1–6
[4] Klepper C. *et al* 2019 Sub-divertor fuel isotopic content detection limit for JET and its impact on ICRF core heating and DTE2 operations *Nucl. Fusion* **60** 016021
[5] Lerche E. *et al* (JET EFDA Contributors) 2011 Optimizing ion-cyclotron resonance frequency heating for ITER: dedicated JET experiments *Plasma Phys. Control. Fusion* **53** 124019
[6] Kruezi U., Jepu I., Sergienko G., Klepper C.C., Delabie E., Vartanian S. and Widdowson A. 2020 Neutral gas analysis for JET DT operation *J. Instrum.* **15** C01032
[7] Mantsinen M. *et al* 2023 Experiments in high-performance JET plasmas in preparation of second harmonic ICRF heating of tritium in ITER *Nucl. Fusion* **63** 112015
[8] Klepper C., Vetter K., Jepu I., Kruezi U., Biewer T., DeVan W., Marcus C. and Mellor R. 2021 Preliminary demonstration on JET of an ITER neutron environment-compatible quadrupole mass-spectrometer *Fusion Eng. Des.* **170** 112672
[9] Vartanian S. *et al* 2021 Simultaneous H/D/T and 3He/4He absolute concentration measurements with an optical Penning gauge on JET *Fusion Eng. Des.* **170** 112511
[10] Marcus C., Biewer T., Jugan A., Klepper C. and Quinlan B. 2024 Eliminating signal bias from vacuum system backstreaming in the ITER diagnostic residual gas analyzer *Proceeding of the 67th Annual Technical Conf. Proceeding* (*Chicago, IL, USA, 6–9, 2024*) (Society of Vacuum Coaters) (https://doi.org/10.14332/svc24.proc.0035)
[11] Jacquet P. *et al* 2024 ICRH operations during the JET tritium and DTE2 campaigns *Nucl. Fusion* **64** 066039
[12] Lennholm M. *et al* (JET contributors, the EUROfusion Tokamak Exploitation Team) 2025 Fusion burn regulation via deuterium tritium mixture control in the joint European Torus *PRX Energy* (https://doi.org/10.1103/PRXEnergy.4.023007)
[13] Lennholm M. *et al* 2017 Real time control developments at JET in preparation for deuterium-tritium operation *Fusion Eng. Des.* **123** 535–40
[14] Piron L. *et al* 2021 Progress in preparing real-time control schemes for deuterium-tritium operation in JET *Fusion Eng. Des.* **166** 112305
[15] Boyer M.D. and Schuster E. 2015 Nonlinear burn condition control in tokamaks using isotopic fuel tailoring *Nucl. Fusion* **55** 083021
[16] Wesson J. 1997 *Tokamaks* 2nd edn (Clarendon)
[17] Joffrin E., Wischmeier M., Hakola A., Tsitrone E., Kappatou A., Vianello N., Baruzzo M., Keeling D. and Labit B. 2024 Overview of the JET last D-T results in support of ITER and the reactor *66th Annual Meeting of the American Physical Society (APS) Division of Plasma Physics* (*Atlanta, Georgia, USA*) (https://meetings.aps.org/Meeting/DPP24/Session/KI03.1)
[18] Boyer M.D. and Schuster E. 2014 Nonlinear control and online optimization of the burn condition in ITER via heating, isotopic fueling and impurity injection *Plasma Phys. Control. Fusion* **56** 104004
[19] Goniche M. *et al* (JET Contributors) 2017 Ion cyclotron resonance heating for tungsten control in various JET H-mode scenarios *Plasma Phys. Control. Fusion* **59** 055001
[20] Van Eester D. *et al* (JET EFDA contributors) 2009 JET (3He)-D scenarios relying on RF heating: survey of selected recent experiments *Plasma Phys. Control. Fusion* **51** 044007
[21] Urbanczyk G. *et al* (the WEST Team) 2021 RF wave coupling, plasma heating and characterization of induced plasma-material interactions in WEST L-mode discharges *Nucl. Fusion* **61** 086027
[22] Eester D.V. and Koch R. 1998 A variational principle for studying fast-wave mode conversion *Plasma Phys. Control. Fusion* **40** 1949
[23] Bosch H.S. and Hale G.M. 1992 Improved formulas for fusion cross-sections and thermal reactivities *Nucl. Fusion* **32** 611–31
[24] Gross R. 1984 *Fusion Energy* (Wiley)
[25] Graber V. and Schuster E. 2020 Nonlinear adaptive burn control and optimal control allocation of over-actuated two-temperature plasmas *2020 American Control Conf. (ACC)* (*Denver, Colorado, 1–3 July 2020*) (https://doi.org/10.23919/ACC45564.2020.9147885) pp 1411–6
[26] Gallart D., Mantsinen M. and Kazakov Y. 2015 Modelling of ICRF heating in DEMO with special emphasis on bulk ion heating *AIP Conf. Proc.* **1689** 060004
[27] Hemsworth R.S. *et al* 2017 Overview of the design of the ITER heating neutral beam injectors *New J. Phys.* **19** 025005
[28] Shimada M. *et al* 2007 Chapter 1: overview and summary *Nucl. Fusion* **47** S1
[29] Khalil H. 2001 *Nonlinear Systems* 3rd edn (Prentice Hall)
[30] Graber V. and Schuster E. 2019 Nonlinear adaptive burn control of two-temperature tokamak plasmas *IEEE Conf. Decision and Control* (*Nice, France, 11–13 December 2019*) (https://doi.org/10.1109/CDC40024.2019.9029943)
[31] Graber V. and Schuster E. 2022 Nonlinear burn control in ITER using adaptive allocation of actuators with uncertain dynamics *Nucl. Fusion* **62** 026016
[32] Graber V., Schuster E., Klepper C., Lerche E., Biewer T. and Lore J. 2025 Burn control in ITER by maximization of ion cyclotron power absorption through regulation of helium-3 concentration *30th IAEA Fusion Energy Conf.* (*Chengdu, People's Republic of China, 13–18 October 2025*) (available at: www.iaea.org/events/fec2025)